

# Coherent bremsstrahlung in a bent crystal

M.V. Bondarenko\*

*Kharkov Institute of Physics and Technology, 1 Academic St., 61108 Kharkov, Ukraine.*

(Dated: April 24, 2019)

Radiation spectrum from high energy  $e^\pm$  in a bent crystal with arbitrary curvature distribution along the longitudinal coordinate is evaluated, based on the stationary phase approximation. For a uniformly bent crystal a closed-form expression for the spectrum is derived. Features such as sharp end of spectrum and volume reflection turnover at beginning of the spectrum are discussed. The coherence length in a bent crystal appears to depend only on the crystal geometry and not on the electron or photon energies, which is essential for interpretation of the results. Estimates of non-dipole radiation and multiple scattering effects are given. The value for the crystal bending angle at which the dipole coherent bremsstrahlung theory holds best appears to be  $\sim 10^{-4}$  rad.

PACS numbers: 29.27.-a, 41.60.-m, 61.80.-x, 78.70.-g

Keywords: bent crystal, continuous potential, coherence length, radiation spectrum

## I. INTRODUCTION

Gamma-radiation emitted by electrons and positrons at their over-barrier motion in bent crystals has been investigated in a few recent experiments [1, 2] searching for signatures of the charged particle volume reflection effect [3] in the radiation spectrum. However, the spectra observed were largely monotonous at typical photon frequencies  $\omega$ , and the difference between the measured spectra from positrons and electrons was basically of the order of the experimental errors. That impedes clear-cut identification of a spectrum region to be associated with volume reflection, since sufficiently high-energy photons should presumably be generated via some simpler mechanism.

In article [4] dedicated to computer modeling of the conditions of experiment [1] it was mentioned that the radiation spectrum must contain the component of so-called coherent bremsstrahlung in a bent crystal (CBBC) (see [5], appendix), arising at fast charged particle highly over-barrier motion, when perturbative treatment of particle interaction with the crystal applies. To say more, this type of radiation may prove even dominant when the crystal bending angle by far exceeds the critical value  $\theta_c$  [22] – then the particle should spend most of its time traveling at angles to active crystal planes much greater than critical, i. e., flying high above the potential barrier. Under those conditions, the frequency of the radiation emitted by the particle at a given instant is proportional to the local frequency of atomic plane crossing by the particle, as in ordinary coherent bremsstrahlung [6]. In course of the particle passage, the angle of atomic plane crossing varies, and thus the coherent radiation intensity sweeps smoothly over the spectrum. Let us point out that CBBC must be present regardless of whether the conditions of volume reflection hold somewhere in the volume of the crystal, i. e., at any ratio of the crystal bending

radius to the critical value  $R_c$  at the given energy.

In view of the described situation, prior to studies of radiation features corresponding to non-perturbative segments of particle motion in bent crystals, it would be appropriate to determine the shape of perturbative CBBC, which provides conceptually the simplest approximation and yields a wide continuous background. Unfortunately, it has not been evaluated completely so far. It is the purpose of the present article to accomplish the relevant calculation, and also to scrutinize the coherence length concept in application to the given case. Secondly, we will assess robustness of the simplest CBBC theory against various deteriorating effects present in nature, such as multiple scattering and the dipole regime failure. It turns out that the range of the dipole CBBC theory is rather limited, although non-vanishing.

In view of the ubiquity of CBBC radiation in bent crystals of various shapes (besides cylindrically bent crystals, in use today are sine-shaped bent crystals [7], other microfabricated configurations may appear), we extend our treatment to the case of arbitrary crystal bend profile. Our ability to cope with it grounds on the applicability of a stationary phase approximation allowing one to treat the crystal curvature as locally constant. That variant of the stationary phase approximation is physically different from that arising in problems of synchrotron-like radiation, and does not contradict to the use of the dipole approximation.

The paper is organized as follows. In Sec. II we define the bent crystal continuous potential and the corresponding transverse force. In Sec. III we proceed to evaluating the particle deflection angle by such a force to the leading order of high-energy perturbation theory of classical mechanics. In Sec. IV we evaluate the radiation spectrum in the dipole approximation, including the quantum effect of radiation recoil (allowing for photon energies to be of the order of initial electron's). In Sec. V the conditions of applicability of such an approximation are analyzed. Sec. VI is a summary.

---

\*Electronic address: bon@kipt.kharkov.ua

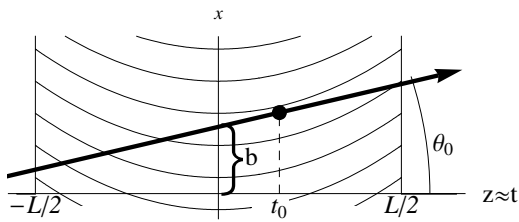


FIG. 1: Schematic of ultra-high-energy particle passage through a thin bent crystal. The point  $t_0$  of tangency to crystal planes gives main contribution to the deflection angle.

## II. CONTINUOUS POTENTIAL OF A WEAKLY BENT PLANARLY ORIENTED CRYSTAL

### A. Geometry definition

At practice, for the coherent bremsstrahlung at over-barrier motion not to be overwhelmed by multiple scattering it is desirable to use a crystal not thicker than a few millimeters (the same situation as with straight crystals). There are various techniques for manufacturing such short bent crystals, but basically they fall into two categories. First – one of the transverse dimensions is made short, and even shorter than longitudinal (i. e.,  $\ll 1$  mm), which permits to bend the crystal along the longitudinal direction [8]. Second – both transverse dimensions are made sufficiently sizeable and the crystal so obtained is bent by some large dimension, but securing that (short) crystallographic planes in the crystal, along which the beam is to be sent, acquire some bending, too. Specifically, the bending of the latter may be achieved through the action of anti-clastic forces, when the crystal is deformed simultaneously by both large dimensions with different strength [9, 10] [23], or one might just arrange the active planes to be under some reasonably small angle  $\alpha$  to the large face, and then they must bend along with the large face, although  $\alpha$  times weaker. At the same time, for issues of particle passage through the crystal deviations of the large crystal faces from planes may be neglected.

For what concerns description of the particle passage, in any case, the geometry implies particle incidence at some (small) angle  $\theta_0$  to  $z$ -axis, chosen normal to the crystal large faces (let the latter be located at positions  $z \approx -L/2$  and  $z \approx L/2$ ) [24], and the particle essentially interacts with the continuous potential of the planes depending only on single coordinate  $x$  (see Fig. 1). The distance between the bent planes is practically unaffected by the crystal curvature, and the equation defining each plane takes the form

$$x_{pl}(z) = C_{pl} + \xi(z), \quad (1)$$

constants  $C_{pl}$  being equal-spaced with the inter-planar distance  $d$ .

Then, if the continuous inter-planar potential in the bent crystal was  $V_{\text{straight}}(x)$  (a periodic function

with period  $d$ ), which corresponds to an acting force  $F_{\text{straight}}(x) = -\frac{\partial V_{\text{straight}}}{\partial x}$ , after bending of this crystal the force will modify to

$$F(x, z) = F_{\text{straight}}(x - \xi(z)) \quad (2)$$

(still, it can be regarded as directed along  $x$ ). For crystals of constant curvature [25],

$$\xi(z) \approx \frac{z^2}{2R}, \quad (3)$$

with  $R = \text{const}$  being the atomic plane bending radius. In what follows, we will rely on the stationary phase approximation, in which the crystal curvature is treated locally, and is described by the local bending radius

$$R(z) = \frac{1}{|\xi''(z)|},$$

to emerge naturally thereafter.

### B. Nearly parabolic continuous potential and the corresponding force

The dynamics of a high-energy particle in a crystal may be described by ultra-relativistic classical mechanics [11]. Also, in the theory of coherent bremsstrahlung it is common to use perturbative description of particle interaction with the crystal, since it offers great simplifications. Conditions of the perturbative description will be specified later (Sec. V).

In the perturbative treatment of classical particle passage dynamics, as well as in quantum theory, it is advantageous to express the periodic continuous potential in form of Fourier series. Such a representation is economic (provided only a few lowest harmonics dominate), and at the same time convenient when proceeding from description of a straight crystal to a bent one. For evaluation of the particle trajectory and the emitted radiation, of direct relevance is not the potential but the force acting on the particle. To define the force – firstly, in a straight crystal – it is convenient to choose the origin of  $x$ -axis in the middle of some inter-plane interval, with respect to which the potential is an even function of  $x$ , whereas the force has to be odd. Then, Fourier decomposition of the force involves sine functions only:

$$F_{\text{straight}}(x) = \sum_{n=1}^{\infty} F_n \sin \frac{2\pi n x}{d}.$$

In the simplest but important case of (110) planar orientation of a crystal with diamond-type lattice (e. g., silicon), the inter-planar continuous potential is approximable by a parabola, and the corresponding force – by a linear-sawtooth function, whose Fourier decomposition

reads

$$\begin{aligned} F_{\text{cool}}^{(110)}(x) &= -\frac{2F_{\text{max}0}}{d}x|_{|x|<d/2} + \text{period.} \\ &= \frac{2F_{\text{max}0}}{\pi} \sum_{n=1}^{\infty} \frac{(-1)^n}{n} \sin \frac{2\pi nx}{d}. \end{aligned} \quad (4)$$

Here  $F_{\text{max}0}$  has the meaning of the force maximal value at zero temperature (at that, the sign of  $F_{\text{max}0}$  equals to that of the particle charge). On the contrary, in another important case of orientation (111), there are two different (but also nearly parabolic) wells within the period of the continuous potential [12], and the force Fourier decomposition turns somewhat more complicated:

$$\begin{aligned} F_{\text{cool}}^{(111)}(x) &= \frac{32}{\pi d} \sum_{n=1}^{\infty} \frac{(-1)^n}{n} \sin \frac{2\pi nx}{d} \\ &\cdot \left\{ \left( \frac{V_L}{3} + V_S \right) \cos \frac{\pi n}{4} - \frac{4}{\pi n} \left( (-1)^n \frac{V_L}{9} + V_S \right) \sin \frac{\pi n}{4} \right\} \end{aligned} \quad (5)$$

( $V_L$  and  $V_S$  have meaning of depths of the alternate unequal potential wells, while their widths  $d_L = \frac{3}{4}d$ ,  $d_S = \frac{1}{4}d$ ). Anyway, once one factors out here the value of the first Fourier coefficient, denoting it as

$$\left( \frac{V_L}{3} + V_S \right) \cos \frac{\pi}{4} + \frac{4}{\pi} \left( \frac{V_L}{9} - V_S \right) \sin \frac{\pi}{4} := \frac{d}{16} F_{\text{max}0}, \quad (6)$$

Eq. (5) will assume a form similar to (4):

$$F_{\text{cool}}^{(111)}(x) = \frac{2F_{\text{max}0}}{\pi} \sum_{n=1}^{\infty} \frac{(-1)^n c_n}{n} \sin \frac{2\pi nx}{d}. \quad (7)$$

Here  $c_n$  is a sequence of coefficients of order unity, neither increasing nor decreasing as  $n \rightarrow \infty$ , and by definition  $c_1 = 1$ . [26]

To take into account thermal smearing of the potential, i. e., force continuity at the locations of atomic planes, the simplest though heuristic trick is to increase the power of  $n$  in the overall  $\frac{1}{n}$  factor of the trigonometric series:

$$\begin{aligned} F_{\text{therm}}(x) &= \frac{2F_{\text{max}0}}{\pi} \sum_{n=1}^{\infty} \frac{(-1)^n c_n}{n^{1+\epsilon}} \sin \frac{2\pi nx}{d}, \\ \epsilon &= \epsilon(T) > 0. \end{aligned} \quad (8)$$

At that, the sequence  $c_n$  (or its parameters  $V_L$ ,  $V_S$ ) may need to be corrected, but still the series is dominated by the first term, for which  $c_1 \approx 1$ . Such a modification acts similarly to the conventional Debye-Waller exponential factor (which, in principle, is also heuristic, only its first order Maclaurin term being rigorously related to thermal averages). We refrain here from discussing the exact relation of  $\epsilon$  with temperature  $T$ , only indicate that for the case of Si (110) at room temperature agreement with the potentials used in the literature is achieved at  $\epsilon \approx 0.4$  (see Fig. 2), whereas for Si (111) it takes  $\epsilon \sim 1$ . To supply

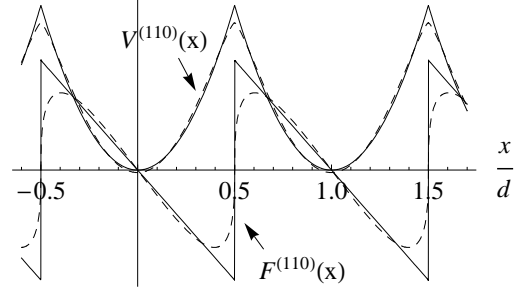


FIG. 2: Inter-planar potential and the corresponding force (Eq. (8)) shapes for positively charged particles in a silicon crystals with (110) orientation. Solid lines:  $\epsilon = 0$  (cooled crystal, Eq. (4)); dashed lines:  $\epsilon = 0.4$  (room-temperature crystal, Eq. (8)). For negatively charged particles the signs of the functions reverse.

more motivation to our ansatz, note that in what follows the summation of series of the type (8) with constant  $\epsilon$  will yield Riemann  $\zeta$ -related functions. Such functions emerge as well for a zero-temperature potential ( $\epsilon = 0$ ), only in that case the function arguments being integer or half-integer. Our approach corresponds to extension of those arguments to arbitrary fractional values, i. e. to an “analytic continuation”, in order to model the effect of the temperature in a simplest way. None of the following numerical results (serving as estimates) depend crucially on this technique.

Practical bent crystals are usually manufactured from silicon. The relevant physical parameters for silicon are

$$d = 1.9 \text{ \AA}, \quad |F_{\text{max}0}| \approx 6 \frac{\text{GeV}}{\text{cm}}, \quad (\text{Si (110)}) \quad (9)$$

$$d = 3.1 \text{ \AA}, \quad |F_{\text{max}0}| \approx 4 \frac{\text{GeV}}{\text{cm}}. \quad (\text{Si (111)}) \quad (10)$$

Note that product  $|F_{\text{max}0}|d$  for those cases has practically identical values, which is important for the subsequent numerical estimates. But all our figures will be drawn only for simpler case (110).

### III. INFINITESIMAL DEFLECTION ANGLE

In this section we will analyze the elastic scattering of ultra-high energy particles by the continuous force defined in the previous section. Choose the time reference point at the moment of particle passage through the middle of the crystal ( $z = 0$ ), so that we may equate  $t \simeq z$  (we will use units  $c = \hbar = 1$ ). Since the beam width in practice is always greater than the inter-planar distance, there is essentially uniform distribution of particles in transverse impact parameters. Defining impact parameter  $b$  of an individual particle as the trajectory initial asymptote intercept on  $x$ -axis, i. e. at  $z = 0$  (see Fig. 1), the force acting on the particle in a bent crystal can be

written as

$$F(t) = \Theta\left(\frac{L}{2} - |t|\right) \frac{2F_{\max 0}}{\pi} \cdot \sum_{n=1}^{\infty} \frac{(-1)^n}{n^{1+\epsilon}} \sin\left(2\pi n \frac{b + \theta_0 t - \xi(t)}{d}\right), \quad (11)$$

with  $\Theta(v)$  – the Heavyside unit step function (zero for negative arguments and unity for positive ones).

First of all, let us evaluate the particle deflection angle. Asymptotically, to leading order in the potential to energy ratio  $V/E$ , the deflection angle is proportional to the integral of force (11) along the unperturbed straight path [27]:

$$\begin{aligned} \theta_{\text{Born}}(\theta_0, b) &= \frac{1}{E} \int_{-L/2}^{L/2} F(t) dt \\ &= \frac{2}{\pi R_c} \sum_{n=1}^{\infty} \frac{(-1)^n c_n}{n^{1+\epsilon}} \cdot \int_{-L/2}^{L/2} \sin\left(2\pi n \frac{b + \theta_0 t - \xi(t)}{d}\right) dt, \end{aligned} \quad (12)$$

where

$$R_c = E/F_{\max 0} \quad (13)$$

is the Tsyganov critical radius [16] (however, our definition of  $R_c$  allows it, along with  $F_{\max 0}$ , to have different sign depending on the particle charge sign). If the crystal bending is macroscopic, in the sense that displacement  $\xi$  of the planes is (generally)  $\gg d$ , the integrand is rapidly oscillatory. For evaluation of such an integral, one may employ the stationary phase approximation [15]. This requires, in the first place, finding stationary phase points  $t_s$  at which

$$t_s(\theta_0) : \quad \theta_0 - \frac{d\xi}{dt} \Big|_{t=t_s} = 0, \quad (14)$$

i. e., the points of tangency of a ray with slope  $\theta_0$  to the family of bent crystalline planes. For a convex function  $\xi$  such a point is unique – and for simplicity we will assume this to be the case, dubbing it  $t_0$  (see Fig. 1). Then, expanding function  $\xi(t)$  in Taylor series about  $t_0$  up to quadratic terms, one brings (12) to the form

$$\begin{aligned} \theta_{\text{Born}}(\theta_0, b) &\approx \frac{2}{\pi R_c} \sum_{n=1}^{\infty} \frac{(-1)^n c_n}{n^{1+\epsilon}} \\ &\cdot \Im \int_{-L/2}^{L/2} dt \exp \left\{ i \frac{2\pi n}{d} (b + \theta_0 t_0 - \xi(t_0) - \frac{1}{2} \xi''(t_0) (t - t_0)^2) \right\}. \end{aligned} \quad (15)$$

Now, if point  $t_0$  belongs to the interval  $-\frac{L}{2} < t_0 < \frac{L}{2}$ , the integral converges in a small vicinity of this point of the width (see a geometric construction in Fig. 3)

$$|t - t_0| \sim l_{\text{SPBC}}(t_0) = \sqrt{2R(t_0(\theta_0))d}, \quad (16)$$

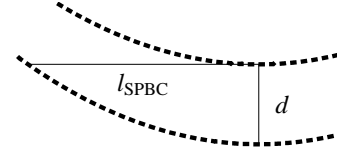


FIG. 3: Geometric interpretation of the coherence length of a fast particle in a bent crystal:  $l_{\text{SPBC}}$  is a half-chord within a curved crystalline plane (radius  $R$ ) tangential to the next curved plane at distance  $d$  from the initial.

where

$$R(t) = \frac{1}{|\xi''(t)|}. \quad (17)$$

Physically, this is the length on which the deflecting external field acts coherently, and will be referred to as coherence length at straight passage through a bent crystal (SPBC). Then, the integration limits in (15) may as well be extended to infinity, and the integral evaluates by a standard formula

$$\int_{-\infty}^{\infty} e^{iAt^2} dt = e^{i\frac{\pi}{4} \text{sgn} A} \sqrt{\frac{\pi}{|A|}}, \quad (\Im m A = 0)$$

with  $\text{sgn}$  function defined as  $\text{sgn} A = -1(+1)$  if  $A < 0 (A > 0)$ . If, on the contrary,  $t_0$  falls beyond the integration interval, the integrand is everywhere rapidly oscillatory, and the result is small (yet there are contributions from the end-points, inferior to those from stationary phase points, which will be neglected throughout for simplicity). With this accuracy,

$$\begin{aligned} \theta_{\text{Born}}(\theta_0, b) &\approx \Theta\left(\frac{L}{2} - |t_0(\theta_0)|\right) \frac{\sqrt{R(t_0(\theta_0))d}}{R_c} \\ &\cdot \frac{2}{\pi} \sum_{n=1}^{\infty} \frac{(-1)^n c_n}{n^{3/2+\epsilon}} \sin\left(-\frac{\pi}{4} \text{sgn} \xi''(t_0(\theta_0))\right. \\ &\quad \left.+ 2\pi n \left[ \frac{b + \theta_0 t_0(\theta_0) - \xi(t_0(\theta_0))}{d} \right] \right). \end{aligned} \quad (18)$$

As for dependencies  $t_0(\theta_0)$ ,  $f(t_0(\theta_0))$ , in case of a crystal of constant curvature (3) they simply express through the only available parameter – the plane bending radius:

$$\begin{aligned} t_0 &= R\theta_0, \quad \xi(t_0) = \frac{R}{2}\theta_0^2, \quad \theta_0 t_0 - \xi(t_0) = \frac{R}{2}\theta_0^2, \\ &\quad (R = \text{const}) \end{aligned}$$

but we do not stick to this case yet.

For the case of orientation (110), when  $c_n \equiv 1$ , the sum in right-hand side of (18) can be expressed in terms

of Hurwitz (generalized Riemann)  $\zeta$ -functions:

$$\begin{aligned} & \frac{2}{\pi} \sum_{n=1}^{\infty} \frac{(-1)^n}{n^{3/2+\epsilon}} \sin \left\{ -\frac{\pi}{4} \text{sgn} \xi''(t_0) + 2\pi n \beta \right\} \\ &= \text{sgn} \xi''(t_0) \frac{2(2\pi)^{\frac{1}{2}+\epsilon}}{\Gamma(\frac{3}{2}+\epsilon)} \\ & \cdot \left( \cos \frac{\pi\epsilon}{2} \zeta \left( -\frac{1}{2} - \epsilon, \left\{ \frac{1}{2} + \beta \text{sgn} \xi''(t_0) \right\} \right) \right. \\ & \left. - \sin \frac{\pi\epsilon}{2} \zeta \left( -\frac{1}{2} - \epsilon, \left\{ \frac{1}{2} - \beta \text{sgn} \xi''(t_0) \right\} \right) \right), \quad (19) \end{aligned}$$

where

$$\beta \left( \frac{b}{d}, \theta_0 \right) = \frac{b + \theta_0 t_0(\theta_0) - \xi(t_0(\theta_0))}{d} \quad (20)$$

characterizes the impact parameter of an oblique trajectory relative to bent planes in point  $z = t_0$ ,  $\zeta(\alpha, v)$  is the Hurwitz zeta-function [17], and braces  $\{\dots\}$  in its second argument indicate the fractional part (ranging from 0 to 1). For orientation (111) the result can be expressed through the Hurwitz zeta-function in a similar manner, but it is somewhat more bulky and shall not be quoted herein.

Function (19) (shown in Fig. 4) is not particularly sensitive to the value of  $\epsilon$ , except around the fracture points. The latter ones are located at

$$\beta = \pm \frac{1}{2}, \pm \frac{3}{2}, \dots \quad (21)$$

In those points, function (19) (and therewith (18)) is extremal and achieves the value

$$\begin{aligned} \max_b \frac{\theta_{\text{Born}}(\theta_0, b)}{\text{sgn} \xi''} &= -\Theta \left( \frac{L}{2} - |t_0(\theta_0)| \right) \\ & \cdot \zeta \left( \frac{3}{2} + \epsilon \right) \frac{\sqrt{2R(t_0(\theta_0))d}}{\pi R_c}, \end{aligned}$$

where  $\zeta(\alpha) = \sum_{n=1}^{\infty} n^{-\alpha}$  is the ordinary Riemann zeta-function. Basically, we see that the magnitude of deflection angles is determined by the crystalline plane curvature radius in the point of tangency to the bent planes.

The noticeable asymmetry of function(s) in Fig. 4 can be traced to the phase shift  $\frac{\pi}{4}$ , arising within the stationary phase approximation. Average value of the deflection angle over impact parameters is strictly zero, as an average of a sum of sine functions over their full period. The physical reason behind that is the uniform distribution of the unperturbed particle flow over the crystal, implying equal influence of positive and negative forces on the entire beam. So, in the considered first order of perturbation theory there is no volume reflection of the beam. Non-zero, however, is the angular spread acquired by the beam, whose measure is the deflection angle mean

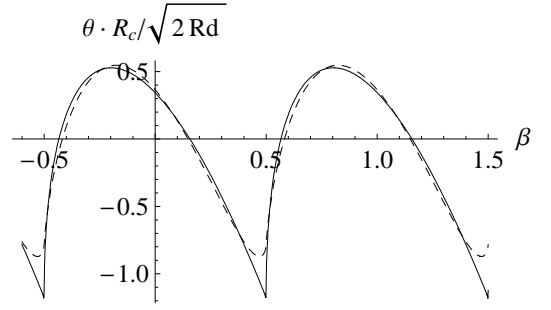


FIG. 4: Deflection angle of a positively charged particle in a bent Si (110) crystal, in units of  $\frac{\sqrt{2Rd}}{R_c}$ , vs. the impact parameter variable  $\beta = \frac{b}{d} + \text{const}$  (see Eq. (20)). Solid line:  $\epsilon = 0$  (cooled crystal), dashed line:  $\epsilon = 0.4$  (room-temperature crystal).

square:

$$\begin{aligned} \langle \theta_{\text{Born}}^2 \rangle &= \frac{1}{d} \int_0^d db \theta^2(\theta_0, b) \\ &\approx \frac{2R(t_0(\theta_0))d}{\pi^2 R_c^2} \sum_{n=1}^{\infty} \frac{c_n^2}{n^{3+2\epsilon}}, \quad (22) \end{aligned}$$

to play an important rôle in the subsequent treatment of radiation.

#### IV. DIPOLE COHERENT BREMSSTRAHLUNG

Having established in the previous section the description of the particle passage through the crystal, we are in a position to calculate the accompanying radiation. As is typical for bremsstrahlung from relativistic particles, the radiation is concentrated within a cone of angles  $\sim \gamma^{-1}$  about the forward direction, and those small angles may be treated inclusively. Let  $\omega$  stand for the photon frequency (energy). Within the dipole approximation, the spectrum of radiation integrated over emission angles, and averaged over the impact parameters  $b$  of particles in the beam, expresses through the acting force as [19]

$$\begin{aligned} \frac{dE_{\text{CBBC}}}{d\omega} &= \frac{e^2 E' \omega}{2\pi E^3} \int_{q_{\min}}^{\infty} \frac{dq}{q^2} \left( 1 + \frac{\omega^2}{2EE'} - \frac{2q_{\min}}{q} + \frac{2q_{\min}^2}{q^2} \right) \\ & \cdot \frac{1}{d} \int_0^d db |F(q, \theta_0, b)|^2 \quad (23) \end{aligned}$$

(cf. [6, 19]). Here

$$E' = E - \omega, \quad q_{\min} = q_{\min}(\omega) = \frac{\omega m^2}{2EE'}, \quad (24)$$

and

$$F(q, \theta_0, b) = \int_{-\infty}^{\infty} dt e^{iqt} F(t, \theta_0, b). \quad (25)$$

Thus,  $q$  is a frequency of the force acting on the particle, and (25) is the Fourier transformation of the intra-crystal force.

With  $F(t)$  given by Eq. (11), its Fourier transform is conveniently evaluated by decomposing the sine function into a pair of exponentials:

$$F(q, \theta_0, b) = \frac{2F_{\max 0}}{\pi} \sum_{n=1}^{\infty} \frac{(-1)^n c_n}{n^{1+2\epsilon}} \cdot \int_{-L/2}^{L/2} dt e^{iqt} \sin\left(2\pi n \frac{b + \theta_0 t - \xi(t)}{d}\right) \\ = \frac{F_{\max 0}}{\pi i} \sum_{n=1}^{\infty} \frac{(-1)^n}{n^{1+\epsilon}} \int_{-L/2}^{L/2} dt \left( e^{i\left(2\pi n \frac{b + \theta_0 t - \xi(t)}{d} + qt\right)} - e^{-i\left(2\pi n \frac{b + \theta_0 t - \xi(t)}{d} - qt\right)} \right). \quad (26)$$

When averaging the square of (26) over the impact parameters, we employ the identity

$$\frac{1}{d} \int_0^d db e^{2\pi i n \frac{b}{d}} e^{-2\pi i m \frac{b}{d}} = \delta_{nm}, \quad (27)$$

which entails

$$\frac{1}{d} \int_0^d db |F(q, \theta_0, b)|^2 \\ = \frac{F_{\max 0}^2}{\pi^2} \sum_{n=1}^{\infty} \frac{c_n^2}{n^{2+2\epsilon}} \left( \left| \int_{-L/2}^{L/2} dt e^{i\left(2\pi n \frac{\theta_0 t - \xi(t)}{d} + qt\right)} \right|^2 + \left| \int_{-L/2}^{L/2} dt e^{i\left(2\pi n \frac{\theta_0 t - \xi(t)}{d} - qt\right)} \right|^2 \right) \quad (28)$$

(note the absence of interference between the exponents after the averaging).

Evaluation of each of the two oscillatory integrals in (28) can proceed via the same stationary phase approximation as in Eq. (15). The external field coherence length is the same as (16), only the location of the stationary-phase point  $t_{n\pm}$ , about which function  $\xi(t)$  has to be Taylor-expanded, now depends on  $\theta_0$  and  $q/n$ . The equations for stationary phase points read

$$t_{n\pm}(q, \theta_0) : \quad \xi'(t_{n\pm}) - \theta_0 = \pm \frac{qd}{2\pi n}. \quad (29)$$

(In accord with (28), radiation from different stationary phase points does not interfere). Physically,  $\xi' - \theta_0$  represents the angle between the beam and the crystalline planes in the stationary phase point. Thereby, Eq. (29) may be viewed as a local coherent bremsstrahlung condition, in which the local frequency of the driving external force is proportional to the local frequency of crystalline plane crossing by the particle, which in turn is proportional to the local angle of the trajectory inclination to the planes (cf. [6]). Ultimately, the approximate

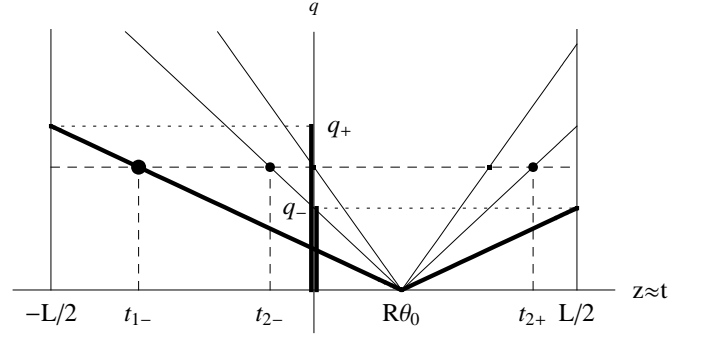


FIG. 5: Local frequencies of plane crossing (thick oblique lines), and the frequencies of higher harmonics (thinner oblique lines), as functions of the particle longitudinal coordinate (time). Drawn for a specific case of crystal with constant curvature, when  $q(t)$  dependences are linear. Vice versa, the construction may be used for determination of stationary phase points for a given frequency (dashed lines). Thick intercepts on the  $q$ -axis schematically show a double-step distribution of the force frequencies described by function  $|F(q)|^2$  (see also Fig. 9b).

$t$ -integration gives

$$\left| \int_{-L/2}^{L/2} dt e^{i\left(2\pi n \frac{\theta_0 t - \xi(t)}{d} \pm qt\right)} \right|^2 \\ \approx \Theta\left(\frac{L}{2} - |t_{n\pm}(q, \theta_0)|\right) \frac{R(t_{n\pm}(q, \theta_0)) d}{n}. \quad (30)$$

Substitution of (28, 30) to (23) leads to the result for the radiation spectrum of coherent bremsstrahlung in a bent crystal:

$$\frac{dE_{\text{CBBC}}}{d\omega} \approx \frac{e^2 F_{\max 0}^2 d E' \omega}{2\pi^3 E^3} \cdot \sum_{n=1}^{\infty} \frac{c_n^2}{n^{3+2\epsilon}} \int_{q_{\min}}^{\infty} \frac{dq}{q^2} \left( 1 + \frac{\omega^2}{2EE'} - \frac{2q_{\min}}{q} + \frac{2q_{\min}^2}{q^2} \right) \\ \cdot \left\{ \Theta\left(\frac{L}{2} - |t_{n+}(q, \theta_0)|\right) R(t_{n+}(q, \theta_0)) + \Theta\left(\frac{L}{2} - |t_{n-}(q, \theta_0)|\right) R(t_{n-}(q, \theta_0)) \right\}. \quad (31)$$

By virtue of the power factor  $\frac{1}{n^{3+2\epsilon}}$ , this sum is strongly dominated by term  $n = 1$ , so the coherent bremsstrahlung spectrum shapes for crystal orientations (110) and (111) appear to be practically the same. In what follows we will concentrate on application of formula (31) to crystals of constant curvature.

For a crystal of constant curvature the solution to Eq. (29) is  $t_{n\pm} = \left(\theta_0 \pm \frac{qd}{2\pi n}\right) R$  (see Fig. 5), and in (31) one may draw constant  $R$  out of the integral, which allows one to accomplish the integration in terms of elementary functions. Introducing parameters

$$q_{\pm} = \frac{2\pi}{d} \left( \frac{L}{2R} \pm |\theta_0| \right) \quad (32)$$

(signifying the frequencies of active crystalline plane crossing at the entrance and at the exit from the crystal) and a function

$$D\left(v, \frac{\omega}{E}\right) = \int_v^1 dy \left(1 + \frac{\omega^2}{2EE'} - 2y + 2y^2\right) \\ = (1-v) \left(\frac{2-v+2v^2}{3} + \frac{\omega^2}{2EE'}\right), \quad (33a)$$

$$\equiv \frac{1}{3} + \frac{1}{2} \left(\frac{1}{2} - v\right) + \frac{2}{3} \left(\frac{1}{2} - v\right)^3 \\ + (1-v) \frac{\omega^2}{2EE'}, \quad (33b)$$

$$(0 \leq v \leq 1)$$

the expression for the radiation spectrum converts to

$$\frac{dE_{\text{CBBC}}}{d\omega} = \frac{e^2 F_{\text{max}0}^2 R d E'^2}{\pi^3 m^2 E^2} \\ \cdot \sum_{n=1}^{\infty} \frac{c_n^2}{n^{3+2\epsilon}} \left\{ \Theta(nq_- - q_{\min}) D\left(\frac{q_{\min}}{nq_-}, \frac{\omega}{E}\right) \right. \\ + \Theta(nq_- + q_{\min}) \Theta(nq_+ - q_{\min}) D\left(\frac{q_{\min}}{nq_+}, \frac{\omega}{E}\right) \\ \left. + \Theta(-nq_- - q_{\min}) \left[ D\left(\frac{q_{\min}}{nq_+}, \frac{\omega}{E}\right) - D\left(\frac{q_{\min}}{n|q_-|}, \frac{\omega}{E}\right) \right] \right\}. \quad (34)$$

The behavior of the spectrum for different incidence angles is illustrated in Figs. 6, 7. Despite being composed of discontinuous  $\Theta$ -functions, in total (34) is everywhere continuous, as is conditioned by its initial integral representation (31). Still, there are discontinuities in the derivative of (34) manifesting themselves as sharp curve breaks (“ankle”-type). Beyond the first two, major breaks [28] (corresponding to  $n = 1$ ) the spectrum effectively ends, and only contributions from higher harmonics remain. Those main “ankles” are located at photon energies

$$\omega_{\pm} = \frac{1}{\frac{1}{E} + \frac{1}{2\gamma^2 |q_{\pm}|}}. \quad (35)$$

Note that when  $|\theta_0|$  is only slightly below  $\frac{L}{2R}$ , then  $\omega_- \ll \omega_+$ , and at  $\omega \leq \omega_-$  the spectrum develops a sharp spike, although superimposed on the background of equal height. That condition corresponds to a trajectory nearly tangential to the crystalline planes at the entrance or exit from the crystal, and although this feature may be of experimental utility, one should beware that our present stationary phase approximation, as well as the dipole approximation itself, are in substantial error there [29].

There are other important features of the CBBC spectrum concerning dependencies on the geometric parameters  $R$ ,  $L$  and  $\theta_0$ :

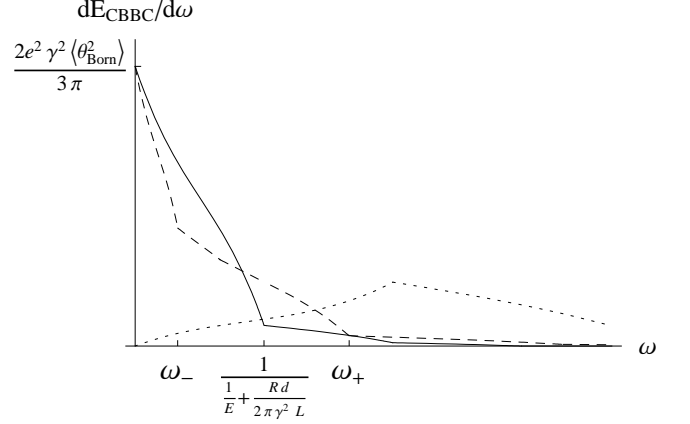


FIG. 6: Radiation spectra neglecting multiple scattering and incoherent bremsstrahlung, for fixed  $\frac{2\pi L\gamma^2}{Rd} \ll E$  and varying  $|\theta_0|$  (temperature effects are practically indistinguishable; the type of crystal orientation, (110) or (111), mainly affects the frequency and intensity scales). Solid line:  $\theta_0 = 0$  ( $\omega_-$  and  $\omega_+$  coincide); dashed:  $|\theta_0| = \frac{L}{3R}$ ; dotted:  $|\theta_0| = \frac{L}{R}$ .

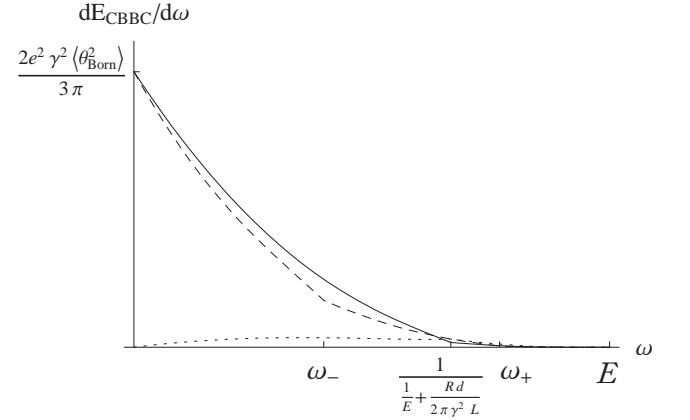


FIG. 7: Same as Fig. 6, for  $\frac{2\pi L\gamma^2}{Rd} = 2E$ . The spectrum shape is strongly influenced by the parabolic factor  $E'^2/E^2$  in (34).

- (i) It is natural that the differential cross-section of coherent radiation is proportional to the square of the field strength and to the square of the coherence length (16). The dependence in (34) on the ratio  $\omega/E$  in the pre-factor and in  $D$ -functions reflects quantum phase space and electron spin effects. We accentuate that the coherence length in our problem is independent of  $\omega$ , the nature of the coherence being entirely due to the coordinate dependence of the external field. The value of the coherence length bears on the magnitude of coherent radiation intensity. In contrast, the photon formation length  $l_{\text{form}} = q_{\min}^{-1} \simeq q_{\pm}^{-1}$  depends on  $\omega$ . It sets the scale of resulting photon energies, correlating with spacings  $q_{\pm}^{-1}$  between the neighboring crystalline planes measured along the particle trajectory at the entrance to and at the exit from the

crystal.

(ii) One can check that as  $\omega \rightarrow 0$  the limit of (31) is

$$\frac{dE_{\text{CBBC}}}{d\omega} \xrightarrow{\omega \rightarrow 0} \frac{2e^2}{3\pi} \gamma^2 \langle \theta_{\text{Born}}^2 \rangle \quad (36)$$

with  $\langle \theta_{\text{Born}}^2 \rangle$  given by Eq. (22). Apparently, this value does not depend on the crystal thickness  $L$ .

(iii) The total radiation energy emitted per one electron

$$E_{\text{CBBC}} = \int_0^E d\omega \frac{dE_{\text{CBBC}}}{d\omega} \quad (37)$$

expresses rather simply and quite differently in two limiting cases: when photon recoil effects are negligible, and when they are decisive. If the “moderately high energy” condition  $2\gamma^2 q_+ \ll E$  is met, then  $q_{\min} \approx \frac{\omega}{2\gamma^2}$  and the second argument of all the  $D$ -functions in (34) may be put to zero. For this case, one finds

$$E_{\text{CBBC}} \simeq L \frac{8e^2}{3\pi^2} \gamma^2 \frac{F_{\max 0}^2}{m^2} \sum_{n=1}^{\infty} \frac{c_n^2}{n^{2+2\epsilon}}. \quad (38)$$

$$\left( \gamma \ll \frac{md}{2\pi} \frac{R}{L} \sim 10^2 \frac{R}{L} \right) \quad (39)$$

In contrast to the differential intensity, the total emitted energy here is proportional not to the square of the coherence length but to the crystal thickness. Remarkably, it does not depend on  $R$  or  $\theta_0$ , and just equals to the total energy of coherent bremsstrahlung radiation in a *straight* crystal of thickness  $L$ .

If the opposite condition  $2\gamma^2 q_+ \gg E$  holds, then the first argument of all the  $D$ -functions in (34) may be put to zero, giving

$$\begin{aligned} E_{\text{CBBC}} &\simeq \left. \frac{dE_{\text{CBBC}}}{d\omega} \right|_{\omega \rightarrow 0} \int_0^E d\omega \frac{E'^2}{E^2} \left( 1 + \frac{3\omega^2}{4EE'} \right) \\ &= E \frac{19e^2}{36\pi^3} \frac{F_{\max 0}^2 R d}{m^2} \sum_{n=1}^{\infty} \frac{c_n^2}{n^{3+2\epsilon}} \Theta \left( \frac{L}{2R} - |\theta_0| \right). \end{aligned} \quad (40)$$

$$\left( \gamma \gg \frac{md}{2\pi} \frac{R}{L} \sim 10^2 \frac{R}{L} \right) \quad (41)$$

So, in this limit even the total radiation energy does not depend on the crystal thickness.

(iv) At

$$|\theta_0| \gg \frac{L}{2R} \quad (42)$$

(a large angle or straight crystal limit), Eqs. (32, 35) yield  $q_- \simeq -q_+ < 0$ ,  $\omega_- \simeq \omega_+$ . Then in

(34) the term with  $\Theta(nq_- - q_{\min})$  vanishes. The next term containing  $\Theta(nq_- + q_{\min})\Theta(nq_+ - q_{\min})$  is non-zero only in relatively small intervals  $n|q_-| \leq q_{\min} < nq_+$ , yet the corresponding  $D$ -function has its first argument close to unity and thereby is small (cf. Eq. (33a)):

$$D\left(\frac{q_{\min}}{nq_+}, \frac{\omega}{E}\right) \simeq \left(1 - \frac{q_{\min}}{nq_+}\right) \left(1 + \frac{\omega^2}{2EE'}\right) \ll 1. \quad (43)$$

Finally, the term containing  $\Theta(-nq_- - q_{\min})$  contributes on the full-fledged interval  $q_{\min} \leq n|q_-|$ , i. e., basically at  $\omega \leq \omega_- \simeq \frac{1}{\frac{1}{E} + \frac{1}{4\pi\gamma^2|\theta_0|}}$ , but there is a valuable cancelation between the corresponding  $D$ -functions:

$$\begin{aligned} &D\left(\frac{q_{\min}}{nq_+}, \frac{\omega}{E}\right) - D\left(\frac{q_{\min}}{n|q_-|}, \frac{\omega}{E}\right) \\ &\simeq \frac{\partial}{\partial v} D\left(v, \frac{\omega}{E}\right) \Big|_{v=\frac{q_{\min}}{n|q_-|}} \frac{q_{\min}}{n} \left( \frac{1}{q_+} - \frac{1}{|q_-|} \right) \\ &\simeq \left( 1 - 2 \frac{q_{\min}}{n|q_-|} + 2 \frac{q_{\min}^2}{n^2|q_-|^2} + \frac{\omega^2}{2EE'} \right) \frac{q_{\min}}{nq_-^2} \frac{2\pi L}{Rd}, \end{aligned} \quad (44)$$

$$|q_-| \simeq \frac{2\pi|\theta_0|}{d}.$$

Therewith, the radiation spectrum reduces to

$$\begin{aligned} \frac{dE}{d\omega} &\simeq L \frac{e^2 F_{\max 0}^2 d^2}{2\pi^4 m^2 \theta_0^2} \frac{E'^2}{E^2} q_{\min} \\ &\cdot \sum_{n=1}^{\infty} \Theta\left(n - \frac{q_{\min}}{|q_-|}\right) \frac{c_n^2}{n^{4+2\epsilon}} \left( 1 - \frac{2q_{\min}}{n|q_-|} + \frac{2q_{\min}^2}{n^2|q_-|^2} + \frac{\omega^2}{2EE'} \right), \end{aligned} \quad (45)$$

which complies with the coherent bremsstrahlung spectrum in a straight crystal [6] (note that dependence on  $R$  drops out). However due to the  $\theta_0^{-2}$  dependence of (45), with the increase of  $|\theta_0|$  to reach (42) the intensity attenuates. Besides that, at large incidence angles the validity of the continuous potential approximation may fail.

## V. CONDITIONS OF APPLICABILITY

Our framework in the preceding two sections had been developed by the principle of maximal theoretical simplicity. In Sec. III, in our infinitesimal description of the particle deflection in the crystal we appealed to the high value of the particle energy. In Sec. IV we yet adopted the dipole approximation to radiation emission, which, however, is known [19] to fail at a sufficiently high energy. Therefore, we have to investigate whether these two approximations are mutually consistent under conditions of a real silicon crystal, and if yes, what is the



domain of their compatibility. Yet, besides the continuous potential influence on the particle there exists incoherent scattering on individual nuclei, which affects the particle deflection as well as radiation. After all, in a case  $R \gg R_c$  the condition of infinitesimal deflection certainly fails in vicinity of the volume reflection point, and that may also affect the radiation spectrum in some frequency domain. The present, last section comprises estimates of all the mentioned effects.

### A. Validity of infinitesimal deflection approximation

The condition of validity of the straight passage approximation is the smallness of the particle transverse displacement relative to the inter-planar distance. Based on Eq. (11), let us evaluate the particle transverse displacement as a function of time:

$$\begin{aligned} \Delta x(t) &= \int_{-L/2}^t dt' \int_{-L/2}^{t'} dt'' \frac{F(t'')}{E} \\ &= \frac{2}{\pi R_c} \sum_{n=1}^{\infty} \frac{(-1)^n c_n}{n^{1+\epsilon}} \\ &\quad \cdot \int_{-L/2}^t dt' \int_{-L/2}^{t'} dt'' \sin \left( 2\pi n \frac{b + \theta_0 t'' - \xi(t'')}{d} \right). \end{aligned} \quad (46)$$

Changing here the order of integrations, and again expanding  $\xi(t'')$  in Taylor series about point  $t_0$ , one converts the double integral in (46) to a single one which is of Fresnel type:

$$\begin{aligned} \frac{\Delta x(t) R_c}{l_{\text{SPBC}}^2} &= \frac{2}{\pi} \sum_{n=1}^{\infty} \frac{(-1)^n c_n}{n^{1+\epsilon}} \\ &\quad \cdot \int_{-\frac{L/2+t_0}{l_{\text{SPBC}}}}^{\frac{t-t_0}{l_{\text{SPBC}}}} d\tau \left( \frac{t-t_0}{l_{\text{SPBC}}} - \tau \right) \sin \{ 2\pi n (\beta - \tau^2) \}. \end{aligned} \quad (47)$$

It behaves as shown in Fig. 8 (by solid line). At large negative  $\frac{t-t_0}{l_{\text{SPBC}}}$

$$\begin{aligned} \frac{\Delta x(t) R_c}{l_{\text{SPBC}}^2} &\stackrel{\frac{t-t_0}{l_{\text{SPBC}}} \gg 1}{\approx} \left( 1 + \frac{t-t_0}{L/2+t_0} \right) \\ &\quad \cdot \frac{1}{2\pi^2} \sum_{n=1}^{\infty} \frac{(-1)^{n-1} c_n}{n^{2+\epsilon}} \cos \left\{ 2\pi n \left( \beta - \frac{(L/2+t_0)^2}{l_{\text{SPBC}}^2} \right) \right\} \\ &\quad + \frac{l_{\text{SPBC}}^2}{8\pi^3 (t-t_0)^2} \sum_{n=1}^{\infty} \frac{(-1)^{n-1} c_n}{n^{3+\epsilon}} \sin \left\{ 2\pi n \left( \beta - \frac{(t-t_0)^2}{l_{\text{SPBC}}^2} \right) \right\}. \end{aligned} \quad (48)$$

A curious feature here is the weak linear drift at the initial stage, visualized in Fig. 8 and represented in Eq. (48)

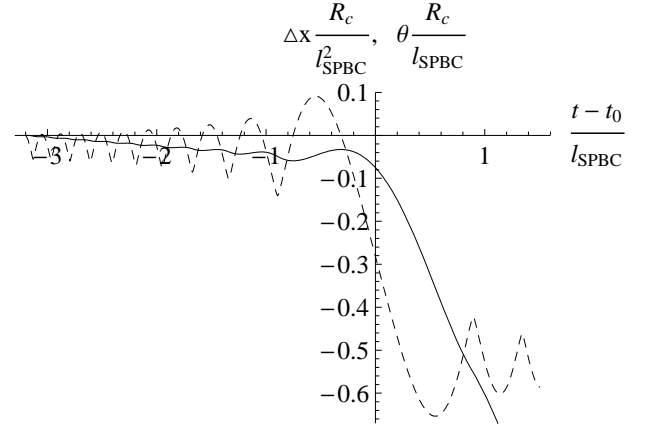


FIG. 8: Local transverse departure from the initial straight trajectory  $\Delta x(t)$ , expressed in units of  $l_{\text{SPBC}}^2/R_c$  (solid line), and the local deflection angle  $\theta(t)$ , in units of  $l_{\text{SPBC}}/R_c$  (dashed line), as functions of the distance to the point of tangency to crystalline bent planes (for some specific impact parameter). Both curves are built for the room-temperature case  $\epsilon = 0.4$ , crystal orientation (110) and for  $\beta = -0.7$  (see Eq. (20)).

by the term proportional to  $1 + \frac{t-t_0}{L/2+t_0}$ . It may be interpreted as beam refraction at the entrance to the bent crystal. The refraction angle sign depends on the impact parameter at the entrance. However, by the absolute magnitude this effect is small, and for our current estimates less relevant.

Most relevant is the behavior of function (47) at  $t > t_0$  where it grows linearly (which corresponds to a motion along the scattering angle final asymptote), as

$$\begin{aligned} \frac{\Delta x(t) R_c}{l_{\text{SPBC}}} &\stackrel{\frac{t-t_0}{l_{\text{SPBC}}} \gg 1}{\approx} (t-t_0) \frac{\sqrt{2}}{\pi} \sum_{n=1}^{\infty} \frac{(-1)^n c_n}{n^{3/2+\epsilon}} \sin \left( 2\pi n \beta - \frac{\pi}{4} \right) \\ &\quad + \frac{1}{2\pi^2} \sum_{n=1}^{\infty} \frac{(-1)^n c_n}{n^{2+n}} \cos \left\{ 2\pi n \left( \beta - \frac{(L/2+t_0)^2}{l_{\text{SPBC}}^2} \right) \right\} \\ &\quad + \frac{l_{\text{SPBC}}^2}{8\pi^3 (t-t_0)^2} \sum_{n=1}^{\infty} \frac{(-1)^{n-1} c_n}{n^{3+\epsilon}} \sin \left\{ 2\pi n \left( \beta - \frac{(t-t_0)^2}{l_{\text{SPBC}}^2} \right) \right\}. \end{aligned} \quad (49)$$

In fact, the acting force contribution builds up only before the particle reaches the final asymptote. For an actual estimate of the transverse displacement up to that moment one may simply take the value of (49) at  $\frac{t-t_0}{l_{\text{SPBC}}} \simeq 1$ . For reliability of the straight passage approximation, the corresponding transverse displacement  $\Delta x$  needs to be less than the inter-planar interval half-width:

$$\Delta x(t_0 + l_{\text{SPBC}}) \ll d/2. \quad (50)$$

With the use of Eq. (49), condition (50) boils down to

$$R \ll \frac{\pi}{4} |R_c|. \quad (\text{for perturb. defl. angle}) \quad (51)$$

This is physically sound, since at  $R \geq R_c$  non-perturbative effects such as planar channeling, or volume reflection in the bent crystal already become important.

Yet, for applicability of the stationary phase approximation the necessary requirement is that the external field coherence length  $l_{\text{SPBC}} = \sqrt{2Rd}$  be small compared to the crystal half-thickness, i. e.,

$$\sqrt{2Rd} \ll L/2. \quad (52)$$

### B. Validity of dipole condition for radiation

Next, let us examine the conditions demanded by our description of radiation. In fact, since we assume the radiation at a given frequency to be generated in a relatively small vicinity of an appropriate (frequency-dependent) point within the crystal, the condition for infinitesimality of the deflection is not (50) but rather  $\text{var } \Delta x(t) \ll d/2$ , where  $\text{var } \Delta x(t)$  is the oscillatory part of the trajectory (apart from the linear, inertial motion causing no radiation) and  $t \sim L/2$  is a generic point within the crystal. Letting in the last line of (48) or of (49)  $|t - t_0| \sim L/2$ , one derives the corresponding requirement

$$\frac{L^2}{R^2} \gg \frac{2\sqrt{2}}{\pi^3} \frac{d}{|R_c|}. \quad (53)$$

Secondly, we had employed dipole approximation for the radiation, which presumes to smallness of the particle deflection angle compared to the typical radiation angle  $\gamma^{-1}$ . So, let us evaluate from Eq. (11) the *local* angle of deflection from the straight path. Using again the stationary phase approximation,

$$\begin{aligned} \theta(t) &= \int_{-L/2}^t dt' \frac{F(t')}{E} \\ &\approx \frac{l_{\text{SPBC}}}{R_c} \frac{2}{\pi} \sum_{n=1}^{\infty} \frac{(-1)^n c_n}{n^{1+\epsilon}} \int_{-\infty}^{t-t_0} d\tau \sin(2\pi n(\beta - \tau^2)). \end{aligned}$$

This is an ordinary Fresnel integral; it is observed to converge within the range  $l_{\text{SPBC}}$ , and its asymptotic forms at  $|t - t_0| \gg l_{\text{SPBC}}$  are [30]

$$\begin{aligned} \theta(t) &\underset{-\frac{t-t_0}{l_{\text{SPBC}}} \ll 1}{\approx} \frac{l_{\text{SPBC}}^2}{R_c(t_0 - t)} \\ &\cdot \frac{1}{2\pi^2} \sum_{n=1}^{\infty} \frac{(-1)^{n-1} c_n}{n^{2+\epsilon}} \cos\left(2\pi n\left(\beta - \frac{(t-t_0)^2}{l_{\text{SPBC}}^2}\right)\right), \end{aligned} \quad (54)$$

and

$$\begin{aligned} \theta(t) &\underset{\frac{t-t_0}{l_{\text{SPBC}}} \gg 1}{\approx} \theta_{\text{Born}} \\ &+ \frac{l_{\text{SPBC}}^2}{R_c(t-t_0)} \frac{1}{2\pi^2} \sum_{n=1}^{\infty} \frac{(-1)^{n-1} c_n}{n^{2+\epsilon}} \cos\left(2\pi n\left(\beta - \frac{(t-t_0)^2}{l_{\text{SPBC}}^2}\right)\right). \end{aligned} \quad (55)$$

Now, for validity in weakly bent crystals of the dipole approximation to radiation, we need smallness of the product  $\text{var } \gamma\theta(t)$  at  $|t - t_0| \lesssim L/2$ . Substituting in Eq. (54) or the last line of Eq. (55)  $|t - t_0| \rightarrow L/2$ , and replacing the sum by its typical value  $1/\sqrt{2}$ , we get

$$\text{var } \gamma\theta|_{|t-t_0| \lesssim L/2} \ll 1 \quad \Rightarrow \quad \frac{L}{R} \gg \tilde{\theta}_V = \frac{2\sqrt{2}|F_{\text{max}0}|d}{\pi^2 m}. \quad (56)$$

Here  $\tilde{\theta}_V$  is a parameter similar to  $\theta_V = \frac{V_0}{m}$  of [19]. [31] With the use of parameters (9), numerically one finds

$$\tilde{\theta}_V \approx 0.65 \cdot 10^{-4} \quad (57)$$

both for Si (110) and Si (111). It is worth emphasizing that in a bent crystal the validity of the dipole approximation to radiation depends on  $\tilde{\theta}_V$  smallness in comparison not with the Lindhard critical angle

$$\theta_c = \sqrt{\frac{d}{2|R_c|}} \quad (58)$$

(dependent on the particle energy via  $R_c$ ), but with the crystal bending angle  $L/R$ .

### C. Influence of multiple scattering on particle deflection and on radiation

#### 1. Deflection

The angle of particle deflection in the continuous potential field also competes with the (rms, plane) angle of multiple scattering. The latter has a square root dependence on the medium thickness traversed [20]:

$$\theta_{\text{mult}}(\Delta t) = \sqrt{\langle \theta_x^2 \rangle_{\text{mult}}} \equiv \sqrt{\frac{1}{2} \langle \theta^2 \rangle_{\text{mult}}} = \frac{1}{\gamma} \sqrt{\frac{\Delta t}{l_{\text{mult}}}}. \quad (59)$$

For *electrons and positrons* in silicon [20]

$$l_{\text{mult}} \approx 0.13 \text{ mm.} \quad (e^{\pm} \text{ in Si}) \quad (60)$$

For multiple scattering not to affect significantly the particle deflection in the target,  $\theta_{\text{mult}}(L)$  must be less than the angle given by Eq. (18):

$$\sqrt{\frac{L}{l_{\text{mult}}}} \ll \frac{|F_{\text{max}0}|\sqrt{Rd}}{m},$$

which entails

$$\frac{L}{R} \ll \left(\frac{F_{\text{max}0}}{m}\right)^2 l_{\text{mult}} d \approx \left\{ \begin{array}{c} 3.6 \\ 2.5 \end{array} \right\} \cdot 10^{-2} \cdot \left\{ \begin{array}{c} \text{Si (110)} \\ \text{Si (111)} \end{array} \right\} \quad (61)$$

## 2. Radiation

Concerning the coherent radiation at typical frequencies, again, condition (61) is not crucial. Instead, one is to compare  $\theta_{\text{mult}}$  with angle  $\text{var } \theta(t)$  at  $|t - t_0| \sim L/2$ . Should we be interested in the radiation angular distribution,  $\theta_{\text{mult}}$  had to be count on the whole crystal thickness  $L$ . However, if only the (angle-integral) radiation spectrum matters, for absence of the multiple scattering influence on it, angle  $\text{var } \theta$  at  $|t - t_0| \sim L/2$  should be large compared to the multiple scattering angle only on length  $l_{\text{SPBC}}$ :

$$\text{var } \theta|_{|t-t_0| \sim L/2} \gg \Delta\theta_{\text{mult}}(l_{\text{SPBC}}), \quad (62)$$

i. e.,

$$\sqrt{\frac{l_{\text{SPBC}}}{l_{\text{mult}}}} \ll \tilde{\theta}_V \frac{R}{L}.$$

For the crystal plane bending angle this implies

$$\frac{L}{R} \ll \tilde{\theta}_V \sqrt{\frac{l_{\text{mult}}}{l_{\text{SPBC}}}} \approx \left\{ \begin{array}{c} 1.7 \\ 1.5 \end{array} \right\} \cdot 10^{-4} \left( \frac{1\text{m}}{R} \right)^{1/4} \cdot \left\{ \begin{array}{c} \text{Si (110)} \\ \text{Si (111)} \end{array} \right\} \quad (63)$$

### D. Incoherent bremsstrahlung background

Still another issue is that the coherent radiation receives a background from incoherent radiation acts. A standard way to estimate the incoherent bremsstrahlung intensity in the crystal is to take the radiation in an amorphous target made of the same material:

$$\frac{dE_{\text{BH}}}{d\omega} = \frac{L}{L_0} \left[ \frac{4}{3} \left( 1 - \frac{\omega}{E} \right) + \frac{\omega^2}{E^2} \right] \Theta(E - \omega). \quad (64)$$

Here  $L_0$  is the radiation length, for silicon amounting [20]

$$L_0 = 9.36 \text{ cm}. \quad (65)$$

The  $\omega$ -dependence of (64) is mild, and as an estimate of  $dE_{\text{BH}}/d\omega$  one may take its value at  $\omega \simeq 0$ .

To compare with, the spectral intensity of the CBBC radiation at an average radiation frequency  $\omega \sim \frac{\omega_+ + \omega_-}{4}$  (see Figs. 6, 7) is about half of its maximal value (36):

$$\left. \frac{dE_{\text{CBBC}}}{d\omega} \right|_{\omega \sim \frac{\omega_+ + \omega_-}{2}} \sim \frac{e^2}{3\pi} \gamma^2 \langle \theta_{\text{Born}}^2 \rangle \quad (66a)$$

$$\equiv \frac{2e^2 F_{\text{max}0}^2 R d}{3\pi^3 m^2} \sum_{n=1}^{\infty} \frac{c_n^2}{n^{3+2\epsilon}}. \quad (66b)$$

$$(|\theta_0| < L/2R)$$

Numerically, Eq. (66b) gives

$$\begin{aligned} \frac{e^2}{3\pi} \gamma^2 \langle \theta_{\text{Born}}^2 \rangle &= \frac{e^2}{3\pi} \left( \frac{F_{\text{max}0} d}{\pi m} \right)^2 \frac{2R}{d} \sum_{n=1}^{\infty} \frac{c_n^2}{n^{3+2\epsilon}} \\ &\approx \left\{ \begin{array}{c} 4.5 \cdot 10^{-4} \\ 3 \cdot 10^{-4} \end{array} \right\} \frac{R}{\text{cm}} \cdot \left\{ \begin{array}{c} \text{Si (110)} \\ \text{Si (111)} \end{array} \right\} \quad (67) \end{aligned}$$

As had been mentioned at the end of Sec. IV, the coherent bremsstrahlung spectral intensity is independent of the crystal thickness  $L$ .

Obviously, for significance of the CBBC radiation, it must exceed the incoherent bremsstrahlung contribution:

$$\frac{dE_{\text{CBBC}}}{d\omega} > \frac{dE_{\text{BH}}}{d\omega}. \quad (68)$$

With (67, 64), it appears that the ratio  $dE_{\text{CBBC}}/dE_{\text{BH}}$  depends only on the ratio  $L/R$ , i. e. on the crystal bending angle, with the proportionality coefficient

$$\frac{dE_{\text{CBBC}}}{dE_{\text{BH}}} \sim 10^{-3} \frac{R}{L}. \quad (69)$$

### E. Radiation at volume reflection (small $\omega$ domain)

We had mentioned in Sec. V B that CBBC mechanism may be responsible for a large part of the radiation spectrum even when condition (51) is violated. In the latter case, the infinitesimal deflection approximation fails for evaluation of the particle final deflection angle, overestimating it, and hence the CBBC formula (34) must overestimate the radiation spectrum at sufficiently small  $\omega$ , where it is proportional to the final deflection angle squared. Let us now gauge the scale of  $\omega$  at which modification of CBBC radiation is needed.

At  $R \gg R_c$  the actual mechanism of particle deflection is volume reflection [3], whereat the magnitude of the deflection angle is of the order of Lindhard's critical angle (58). The contributing  $q$ -frequencies of particle oscillation during the volume reflection are effectively *bounded from below* [32] by the value equal to *twice* the channeling frequency  $1/\tau$ :

$$q \geq q_{\text{v.r.}} = \frac{2}{\tau}, \quad (70)$$

with

$$\tau = \tau_+ = \sqrt{\frac{2}{R_c d}} \quad (\text{pos. char. part.}) \quad (71a)$$

$$\tau \simeq \tau_- = \tau_+ \frac{\ln \frac{R}{R_c}}{2\pi} \quad (\text{neg. char. part.}) \quad (71b)$$

(see Fig. 9c). A mode void below frequency (70) arises because in the vicinity of the volume reflection point  $t = t_{\text{refl}}$  (the closest approach to the axis of the crystal bending) the particle moves in each interval nearly by the channeling *half* period of the maximal amplitude, passing through the potential maxima at a nearly grazing angle (see Figs. 9a,b) [33]. As a consequence, at radiation frequency

$$\omega_{\text{v.r.}} = \frac{1}{\frac{1}{E} + \frac{1}{2\gamma^2 q_{\text{v.r.}}}} \quad (72)$$

the spectral intensity  $dE_{\text{coh}}/d\omega$  related with  $|F(q)|^2$  by Eq. (23), must have a turnover (see Fig. 10), and drop

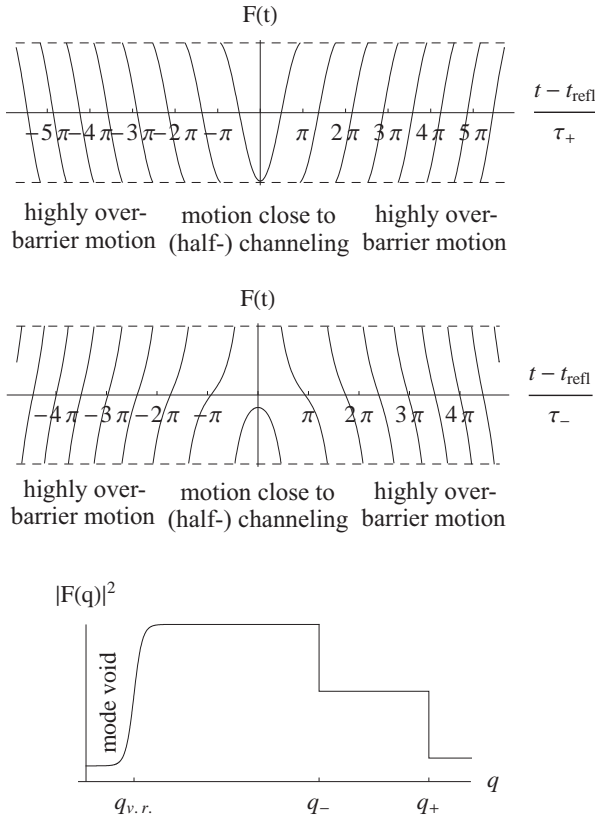


FIG. 9: (a) – exemplary graph of time-dependence of the force acting on the crystal on a (positively) charged particle around the volume reflection point, at  $R \gg R_c$  (the figure corresponds to  $R = 50R_c$ ). The force discontinuities correspond to the particle passage through (sharp) potential maxima at the atomic plane positions. In vicinity of point  $t = t_{\text{refl}}$  the trajectory draws nearly tangential to the maximum potential ridge, and in that sense is close to (half-) channeling. (b) – the same for negatively charged particles. The effective potential maximum is regular ( $F \approx 0$ ) and is situated approximately midway the atomic planes. (c) – schematic of the force Fourier transform modulus square. The dominant contribution to  $|F(q)|^2$  and therethrough to  $dE_{\text{coh}}/d\omega$  comes from the interval  $q_{v.r.} \leq q \leq q_+$ .

at  $\omega \rightarrow 0$  to  $\frac{2e^2}{3\pi}\gamma^2\theta_{v.r.}^2$ . (with  $\theta_{v.r.}^2 < \langle \theta_{\text{Born}}^2 \rangle$ , see Eq. (74) below) [18].

So, the volume reflection effect on the radiation is of purely suppressive, not enhancing character. It stems from the particle inability to sustain in a strong inter-crystalline field a quasi-periodic motion at too low frequencies. Obviously, an over-barrier particle can not spend in an inter-planar channel a time longer than the channeling period (actually, half period).

For the perturbative CBBC theory to have a significant applicability domain, frequency  $\omega_{v.r.}$  must be much lower than the CBBC spectrum end-point  $\omega_+$ , which implies

$$q_{v.r.} \ll \frac{\pi L}{Rd}, \frac{m}{2\gamma}. \quad (73)$$

Condition  $q_{v.r.} \ll \frac{m}{2\gamma}$  results in requirement  $E \ll 10 \text{ TeV}$ ,

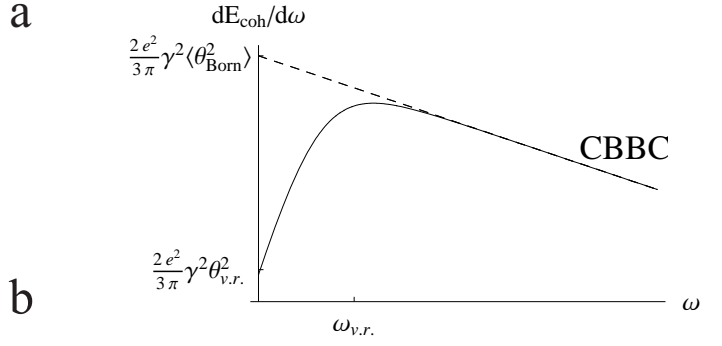


FIG. 10: Schematic of a turnover in the coherent radiation spectrum due to the volume reflection.

which is guaranteed by present accelerator capabilities, whereas condition  $q_{v.r.} \ll \frac{\pi L}{Rd}$ , basically, coincides with (53). The latter may also be regarded as a condition for the particle energy (see Eq. (82) below), which is, however, not very demanding. So, under the conditions of dipole radiation volume reflection effects should manifest themselves in a minor region of the spectrum.

It is yet relevant to estimate the relative depth of the volume reflection dip. The actual value of the volume reflection angle is  $|\theta_{v.r.}| \approx \frac{\pi}{2}\theta_c$  for positively charged, and  $|\theta_{v.r.}| \approx \theta_c$  for negatively charged particles [21]. Therefore,

$$\frac{dE_{v.r.}(0)}{dE_{\text{CBBC}}(\simeq 0)} = \left\{ \begin{array}{c} (\pi/2)^2 \\ 1 \end{array} \right\} \frac{\theta_c^2}{\langle \theta_{\text{Born}}^2 \rangle} \approx \left\{ \begin{array}{c} 6 \\ 2.5 \end{array} \right\} \frac{|R_c|}{R}. \quad (74)$$

$\left\{ \begin{array}{c} \text{pos. char. part.} \\ \text{neg. char. part.} \end{array} \right\}$

Thus, for the turnover to be well discernible, one actually needs  $R$  to be at least a few times larger than  $R_c$ .

## F. Crystal optimal parameters

Let us now assemble conditions (52, 53, 56, 63, 68) and examine their mutual compatibility, the variable parameters being  $R$  and  $L$ . Eqs. (56, 63) together read

$$\tilde{\theta}_V \ll \frac{L}{R} \ll \tilde{\theta}_V \sqrt{\frac{l_{\text{mult}}}{l_{\text{SPBC}}}}, \quad (75)$$

which imply

$$\sqrt{l_{\text{mult}}/l_{\text{SPBC}}} \gg 1. \quad (76)$$

This is reminiscent of the LPM condition

$$l_{\text{form}} \ll l_{\text{mult}}, \quad (77)$$

but at typical radiation frequencies  $l_{\text{form}} \simeq 2q_{\pm}^{-1} \sim 2\frac{Rd}{\pi L}$ , and according to inequality (52), then,  $l_{\text{form}} \ll l_{\text{SPBC}}$ . So, the LPM condition appears to be less crucial than (76).

For fulfilment of condition (76), with  $l_{\text{mult}}$  fixed, one needs to have  $l_{\text{SPBC}}$ , i. e.  $R$  and  $d$ , as low as possible. Note that the value of  $d$  is lower for orientation (110) than for (111), thus orientation (110) is more beneficial. But as for  $R$ , at practice it is normally at least in the range of decimeters, which gives  $\sqrt{l_{\text{mult}}/l_{\text{SPBC}}} \simeq 4$ , and at highest  $R \sim 10$  m one has  $\sqrt{l_{\text{mult}}/l_{\text{SPBC}}} \simeq 1.4$ . Thus, unfortunately, it is impossible to demand inequality (76) as really strong. Anyway, the optimal value for the active crystalline plane bending angle is about

$$\frac{L}{R} \sim \tilde{\theta}_V \left( \frac{l_{\text{mult}}}{l_{\text{SPBC}}} \right)^{1/4} \sim 1.3 \cdot 10^{-4}. \quad (\text{optimal}) \quad (78)$$

Then, the parameter of radiation non-dipoleness (also known as  $\rho$ -parameter [19]) is

$$\gamma\theta|_{|t-t_0| \sim L/2} \sim \tilde{\theta}_V \frac{R}{L} \simeq 0.5, \quad (79)$$

whereas the parameter of radiation decoherence due to multiple scattering is about the same:

$$\frac{\Delta\theta_{\text{mult}}(l_{\text{SPBC}})}{\theta|_{|t-t_0| \sim L/2}} \sim \frac{R}{\tilde{\theta}_V L} \sqrt{\frac{l_{\text{SPBC}}}{l_{\text{mult}}}} \approx 0.5. \quad (80)$$

In view of the narrowness of condition (76), it seems reasonable to suggest that since the size of the coherence length remains the same for all points within the crystal, and the length  $l_{\text{mult}}$  is constant as well, then even if condition (63) fails (multiple scattering effects are substantial), the spectrum *shape* may still be roughly described by the present theory, only the intensity being suppressed by a factor depending on the ratio  $l_{\text{SPBC}}/l_{\text{mult}}$ . However, evaluation of this factor is beyond the scope of the present paper.

In the present context, presuming all abovementioned conditions to be fulfilled, let us check the last crucial condition (68). With (78), ratio (69) will amount  $dE_{\text{CBBC}}/dE_{\text{BH}} \sim 7$ , which is satisfactorily high.

Other relevant conditions (52, 53) are rather easy to fulfil. At bending angle (78) Eq. (52) demands for the crystal thickness

$$\frac{L}{d} \gg \frac{8R}{L} \sim 10^5, \quad L \gg 30 \mu\text{m}. \quad (81)$$

Eq. (53) together with (78) sets the lower bound for the electron energy:

$$E \gg \frac{2\sqrt{2}}{\pi^3} \frac{R^2}{L^2} |F_{\text{max}0}| d \sim 1 \text{GeV}. \quad (82)$$

## VI. SUMMARY AND DISCUSSION

The present study substantiates the notion that spectral intensity of radiation from ultra-high-energy elec-

trons/positrons in a bent crystal is a sum of contributions from particle motion intervals on which the local angle between the particle velocity and the bent crystalline planes is definite, and so each such contribution is similar to coherent bremsstrahlung in a straight crystal. The length of an elementary coherence interval is  $\simeq l_{\text{SPBC}} = \sqrt{2Rd}$ , and so (i) the crystal must be much thicker than that (Eq. (52)); (ii) the radiation spectral intensity (Eqs. (31-34)) is proportional to  $l_{\text{SPBC}}^2 \propto Rd$ , and does not depend on the crystal thickness. Still, under the “moderately high energy” condition (39) the crystal thickness determines the spectrum extent, and thereby, the total energy emitted.

The characteristic feature of CBBC from a perfectly collimated electron beam is the sharp end of the radiation spectrum, whose position depends on the crystal bending angle  $L/R$ . At an angle of electron incidence on the crystal comparable to  $L/2R$  this end of the spectrum splits into a pair of breaks (see Fig. 6). That feature may in principle be experimentally verified with a sufficiently well collimated initial beam.

We have also qualitatively discussed the modification of the coherent radiation spectrum in the domain of small  $\omega$  owing to the onset of the volume reflection phenomenon possible when  $R \gg R_c$ . This modification is of purely suppressive character and manifests itself as a dip at the beginning of the spectrum. There appears to be a maximum in the spectrum around frequency (72), but it is not to be interpreted as a resonance.

The theoretical description adopted in this article had resorted to many simplifications – it did not properly incorporate the temperature dependence of the potential, neglected multiple scattering, and relied on an infinitesimal approximation to the particle deflection (in the bulk of the medium) as well as on a dipole description of the radiation. Conditions (52, 78-82) under which those approximations hold, altogether appear to be restrictive for the crystal bending angle  $L/R$  (see Eq. (78)), so generalization to a non-dipole treatment, and an account of the multiple scattering would be highly desirable. Nonetheless, let us mention that the dipole CBBC conditions are quite nicely met, e. g., in recent experiment [2]. Comparison of the CBBC theory with the experimental data will be given elsewhere.

In conclusion, let us remark that although our paper presumed dependence of the crystal deformation only on one, longitudinal, coordinate, in principle higher-dimensional deformation cases are conceivable, emerging under application of torsion, or owing to intrinsic crystal mosaicity. In those cases the stationary phase approximation must still be applicable, but the description should inevitably become more sophisticated.

**Acknowledgements.** The author wishes to thank A. V. Shchagin for fruitful discussions.

- 
- [1] A. G. Afonin *et al.*, JETP Lett. **88** (2008) 414.
- [2] W. Scandale *et al.*, Phys. Rev. A **79** (2009) 012903.
- [3] A. M. Taratin and S. A. Vorobiev, NIMB **26** (1987) 512.
- [4] Yu. A. Chesnokov, V. I. Kotov, V. A. Maisheev, and I. A. Yazynin, JINST **3** (2008) P02005.
- [5] V. A. Arutyunov, N. A. Kudryashov, V. M. Samconov, and M. N. Strikhanov, Nucl. Phys. B **363** (1991) 283.
- [6] G. Diambri Palazzi, Rev. Mod. Phys. **40** (1968) 611; M. L. Ter-Mikayelyan. High Energy Electromagnetic Processes in Condensed Media, Wiley, New York, 1972.
- [7] V. G. Baryshevsky, I. Ya. Dubovskaya, and A. O. Grubich, Phys. Lett. A **77** (1980) 61; V. V. Kaplin, S. V. Plotnikov, and S. A. Vorob'ev, Zh. Tekh. Fiz. **50** (1980) 1079; S. Bellucci *et al.* Phys. Rev. ST **7** (2004) 023501; A. V. Korol, A. V. Solov'yov, and W. Greiner, Int. J. Mod. Phys. E **13** (2004) 867; N. F. Shul'ga, V. V. Boyko, and A. S. Esaulov, Phys. Lett. A **372** (2008) 2065.
- [8] S. Bellucci *et al.*, Phys. Rev. Lett. **90** (2003) 034801.
- [9] Yu. M. Ivanov *et al.*, JETP Lett. **81** (2005) 99.
- [10] V. Guidi, A. Mazzolari, D. De Salvador, and A. Carnera, J. Phys. D **42** (2009) 182005; S. G. Lekhnitskii. Theory of Elasticity of an Anisotropic Body. Mir, Paris, 1981.
- [11] J. Lindhard, Mat. fys. medd. Kgl. Danske vid. Selskab. **34** (1965) 14.
- [12] V. M. Biryukov, Yu. A. Chesnokov, and V. I. Kotov, Sov. Phys. Usp. **37** (1994) 937.
- [13] A. M. Taratin, Phys. Part. Nucl. **29** (1998) 437; A. M. Taratin and W. Scandale, NIMB **262** (2007) 340.
- [14] V. A. Maisheev, Phys. Rev. ST **10** (2007) 084701.
- [15] F. W. J. Olver. Asymptotics and Special Functions. Academic Press, New York, 1974.
- [16] E. N. Tsyganov, Fermilab Report No. TM-682, 1976 (unpublished); Fermilab Report No. TM-684, 1976 (unpublished).
- [17] T. M. Apostol. Introduction to Analytic Number Theory. Springer, New York, 1976.
- [18] L. D. Landau and E. M. Lifshitz. The Classical Theory of Fields. Pergamon, London, 1962.
- [19] V. N. Baier, V. M. Katkov, and V. M. Strakhovenko. Electromagnetic processes at high energies in oriented single crystals. World Scientific, Singapore, 1998.
- [20] B. Rossi. High Energy Particles. Prentice-Hall, New York, 1952; C. Amsler *et al.* [Particle Data Group], Phys. Lett. B **667** (2008) 1.
- [21] M. V. Bondarenko, arXiv:0911.0107.
- [22] In experiments [1, 2] it takes on values  $3.5 \theta_c$  and  $6 \theta_c$ . This may be not really huge, but for simplicity we will be thinking of a case when that condition holds well.
- [23] In [9] it has been asserted that this technique fails with (110) planar orientation, but works best with (111). Thus, we find it necessary in our article to discuss cases of (110) and (111) in parallel.
- [24] We may treat the crystal faces as planes, although in actual practice, their curvature may be stronger than the curvature of the active crystallographic planes (see, e. g., [10]). The only requirement here is that the face coordinate variation was  $\ll L$  on the width of the beam  $D_{\text{beam}}/2$ , i. e.,  $\frac{D_{\text{beam}}^2}{8R_x} \ll \frac{L}{2}$ . At practice, that condition is usually well satisfied.
- [25] In cases when the active crystal plane bending is achieved due to secondary elastic (quasimosaic) effects, the quadratic approximation for  $\xi$  may be even more accurate than that of a circular arc. The author acknowledges communication with V. Guidi on this point.
- [26] Taking  $V_L \approx 26.5\text{eV}$ ,  $V_S \approx 7.5\text{eV}$ , one obtains  $c_2 = -0.9$ ,  $c_3 = -1.7$ ,  $c_4 = -2.2$ ,  $c_5 = -1.4$ .
- [27] Thereby, it can also be regarded as first Born approximation in coupling with the crystalline field.
- [28] They may coalesce into one if  $\theta_0 \rightarrow 0$ .
- [29] It demands an appropriate account of end-point contributions, with the employment of Fresnel functions.
- [30] It is apparent that (54) is basically a derivative of (48).
- [31] For a parabolic potential,  $V_0 = F_{\text{max}0}d/4$ , which implies  $\tilde{\theta}_V = \frac{8\sqrt{2}}{\pi^2}\theta_V \approx 1.1\theta_V$ . Thus, the difference between the definitions  $\theta_V$  and  $\tilde{\theta}_V$  is inessential.
- [32] Apart from a small, nearly constant contribution from the finite total deflection angle.
- [33] The particle also makes one nearly full undulation period, containing the point  $t = t_{\text{ref}}$ , but alone it can not give radiation competing with coherent radiation from several half-periods. Rather, this single nearly full period may be regarded as transition from one semi-channeled motion to another, standing in antiphase, and no interference of radiation from such antiphased trajectory parts being possible, despite their identical periods.